Physical Mechanism and Theoretical Foundation of Ambient RF Power Harvesting Using Zero-Bias Diodes

Carlos Henrique Petzl Lorenz, Simon Hemour, Ke Wu

Physical Mechanism and Theoretical Foundation of Ambient RF Power Harvesting Using Zero-Bias Diodes

Carlos Henrique Petzl Lorenz, Simon Hemour, *Senior Member, IEEE*, and Ke Wu, *Fellow, IEEE*

***Abstract*— Estimating the amount of harvestable ambient RF and microwave power from the omnipresent electromagnetic sources is of vital importance when designing a wireless device that makes use of ambient microwave power harvesting (AMPH) as a power source. This paper studies and looks into the underlying RF and microwave rectification mechanism at low input ambient power levels, specifically −30 dBm and below. A fundamental theory is formulated and developed, which is able to correctly predict the efficiency of a rectifier including the effects of matching network insertion losses through an easy-to-understand analytical model. The suggested model provides a direct design guideline in determining and choosing the optimal diode for a predetermined application. Based on the developed theoretical framework, the diode characteristics that have a direct impact on the microwave power conversion efficiency are discussed in detail. Three different Schottky diode rectifiers were designed on the basis of the tools described in this paper, thereby validating the proposed model and highlighting the influence of critical diode parameters on its performances. The measured results are then compared with those predicted by the proposed model and state-of-the-art microwave power rectifiers, showing a good model accuracy and also a 10% improvement in the rectifying efficiency for the low input power levels of interest.**

***Index Terms*— Ambient energy harvesting, rectenna, rectifier, RF and microwave power transmission, Schottky diodes.**

I. Introduction

THE use of RF and microwaves to transmit and receive electrical energy has already been successfully demonstrated by Brown [1] and Dickinson [2], following the early attempts of N. Tesla. Those early wireless experiments reached maximum RF-to-dc power conversion eff ciencies of 82.5% for nearly 8 W of input power [2]. However, a good eff ciency was not possible at lower input power levels because of the limitation of technologies available at that time. Improvements in Schottky diode technology have led to an increased RF-to-dc power conversion eff ciency (PCE) at lower input powers [3], approaching 5% at a −30-dBm input power and 40% at −10 dBm or 70% at a 10-dBm input power [4]. Recent progress on the development and deployment of heterojunction backward diodes has made the ambient microwave power harvesting (AMPH) a closer reality by outperforming Schottky diodes, with a PCE of 18%, measured at a −30-dBm input power, and a theoretical eff ciency of almost 40% at the same input power level if matching network insertion losses were eliminated from the circuit [5]. This considerable difference verifie between the maximum calculated PCE in a lossless circuit and the real obtainable PCE, which is reduced because of the matching network insertion losses, is one of the fundamental limitations in the design and development of AMPH devices; the topics further explored and investigated in this paper.

As AMPH generally occurs in a power range below −30 dBm, which can be considered as the peak available power for the AMPH in urban environments [6], [7]. With the ever-decreasing power consumption of electronic components and devices, as described by Koomey *et al.*'s law [8], [9], AMPH becomes an interesting power source for driving the operation of low-power distributed wireless devices, such as sensor or actuator nodes, in distributed wireless networks, as proposed in the Internet of Things schemes, body area networks, and building automation and structure monitoring schemes [7]. Some examples of the proposed applications include the health monitoring of bridges and buildings using batteryless sensors embedded into the structure, and distributed wireless sensor systems to monitor air, water, and noise pollution in cities, just to cite a few [10].

Given the typical low peak power densities that take place in AMPH applications, the analysis presented in this paper will focus on a description of the rectificati n mechanisms over the power range going up to a few microwatts of input power. After depicting the specificitie of Schottky diode microwave rectifier , the effects of matching network insertion losses on the PCE is studied and modeled mathematically. The microwatt model is subsequently extended to the case of higher power levels using a pregenerated deviation matrix.

After the theory presentation, this paper exemplifie the use of the proposed model to determine the optimum Schottky diode and synthesize an AMPH device exploring the

Manuscript received September 9, 2015; revised March 16, 2016 and May 5, 2016; accepted May 16, 2016. This work was supported in part by the Natural Sciences and Engineering Research Council of Canada (NSERC) and by the NSERC-CREATE PERSWADE Training Program.

C. H. P. Lorenz was with the Center for Radiofrequency Electronics Research (CREER) of Quebec and the Poly-Grames Research Center, Department of Electrical Engineering, Ecole Polytechnique de Montreal, Montreal, QC H3T 1J4, Canada (e-mail: carlos.lorenz@polymtl.ca).

S. Hemour was with the Center for Radiofrequency Electronics Research (CREER) of Quebec and the Poly-Grames Research Center, Department of Electrical Engineering, Ecole Polytechnique de Montreal, Montreal, QC H3T 1J4, Canada. He is now with CNRS and the IMS research center, Department of Science and Technology, University of Bordeaux, F-Talence 33 405, France (e-mail: s.hemour@ieee.org).

K. Wu is with the Center for Radiofrequency Electronics Research (CREER) of Quebec and the Poly-Grames Research Center, Department of Electrical Engineering, Ecole Polytechnique de Montreal, Montreal, QC H3T 1J4, Canada (e-mail: ke.wu@polymtl.ca).

Color versions of one or more of the f gures in this paper are available online at http://ieeexplore.ieee.org.

Digital Object Identifie 10.1109/TMTT.2016.2574848

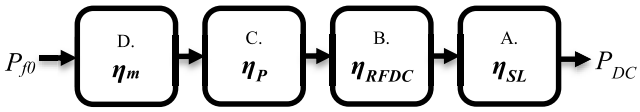

Fig. 1. Microwave power rectif cation eff ciency chain.

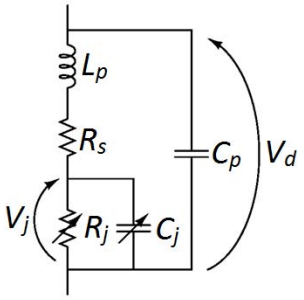

Fig. 2. Diode model considered in the developments described in this paper.

GSM-1900 frequency band. Off-the-shelf Schottky diodes are evaluated using the proposed methodology to estimate the maximum PCE that each diode is able to provide for a matched input and a given output load. This information together with a study on the maximum attainable matched bandwidth is used to def ne which prototypes are built and evaluated. Finally, the measured RF-to-dc PCE of three selected prototypes is presented and compared with the state-of-the-art published results, simulation results, and the theoretical model predictions. A very good agreement between the simulated, predicted, and measured results is shown.

To conclude, a comparison between the proposed and previously published models is made, thus discussing the advantages and disadvantages of each method.

II. Power Conversion Efficiency Chain

To simplify the understanding of the various power loss mechanisms that take place in the process of microwave power rectificati n, the eff ciency chain shown in the following is used [4]. It is important to note that single diode parameters may have an impact on separate blocks in a different manner. This work will focus on rectifie s using a single nonlinear rectificatio device, as in power-scarce applications such as AMPH, adding nonlinear devices would decrease the overall rectifie efficien y, given that parasitic components would be added and the RF-to-dc PCE given in (5) would decrease.

In Fig. 1, η_m stands for the matching eff ciency, η_p for the diode's parasitic efficie cy, η_{RFDC} for the RF-to-dc PCE, and η_{SL} for the dc source-to-load power transfer efficien y. The letters refer to the subsections of this item where the theoretical modeling of each block is developed and presented. The diode's mathematical modeling focuses on η_p, η_{RFDC}, and η_{SL} while the matching eff ciency η_m will later be discussed from both the maximum bandwidth and matching network insertion losses perspectives. It is shown in this work that the matching network insertion loss is of major importance when determining the optimum operation point of a microwave power harvester (MPH). This will be discussed in detail during the development of the mathematical model used to predict η_m as a function of the diode parameters, and this is the f rst time that a matching network loss modeling is introduced for MPH applications.

The Shockley diode model with added packaging parasitic components presented in Fig. 2 is considered during the development done in this work [11]. In this model, R_s is the series linear resistance, R_j is the nonlinear junction resistance whose current can be calculated using (1) [12], C_j is the nonlinear junction capacitance, and C_p and L_p are the packaging parasitic capacitance and inductance, respectively. The packaging parasitic components are only considered in the matching calculations. Although C_j may be bias dependent, it is considered to be constant for the low-power evaluation described in this work

$$I_j(V_j) = I_s\left(e^{\frac{V_j}{N\cdot V_T}} - 1\right) \tag{1}$$

where $V_T = k \cdot T/q$ is the thermal voltage, N is the diode's ideality factor, q is the electron charge, k is the Boltzmann constant, T is the temperature of operation, I_s is the diode's reverse saturation current, and V_j is the voltage applied to the diode's junction.

A. DC Source-to-Load Power Transfer Eff ciency

The dc power transfer efficien y is calculated with the diode's junction acting as a dc generator, with the diode junction resistance $R_j(I_{\mathrm{load}})$ being a Thévenin/Norton resistance [4]

$$\eta_{\mathrm{SL}} = \frac{P_{\mathrm{load}}}{P_{DC}} = \frac{R_L}{R_L + R_s + R_j(I_{\mathrm{load}})}. \tag{2}$$

B. RF-to-DC Power Conversion Effic ency

Most of the published RF and MPH models, which describe the RF-to-dc PCE, consider the diode as a perfect switch whose impedance approaches R_S, the diode's series resistance when directly polarized, and infi ity when reversely polarized [11], [13]. This method delivers good results when the input signal is relatively large, usually in the milliwatt range and above, and the investigated diode has a high barrier leading to a large zero-bias resistance (ZBR) R_{j0}. However, this method does not hold for very low input power levels or for low barrier diodes that present a small ZBR on the order of tens of kiloohms and below.

To model this nonlinearity of R_j, the nonlinear junction current responsivity $\Re_{I0}$ will be used in this work. The current responsivity is def ned as the ratio between the output dc current $I_{j\mathrm{DC}}$ and the input RF power P_{f0} [12] for a 0-Ω load

$$\Re_I = I_{j\mathrm{DC}}/P_{f0}. \tag{3}$$

The usual derivations of $\Re_{I0}$, however, may only be used in the diode's square-law region [4]. Thus, an extended version of the current responsivity will be used, which is denoted in this work by $\Re_I^*$ and may be used out of the diode's square-law region

$$\Re_I^* = \Re_{I_0} \cdot \Delta_{\Re} \tag{4}$$

where $\Re_{I_0} = 1/2 \cdot N \cdot V_T$ and $\Delta_{\Re} = f(V_{jf0}, R_L/R_{j0})$. This extended responsivity equation results from the current–voltage relationship given in (1). What is remarkable about (4) is that the only intrinsic diode characteristic having an impact on the current responsivity is N, the diode's ideality

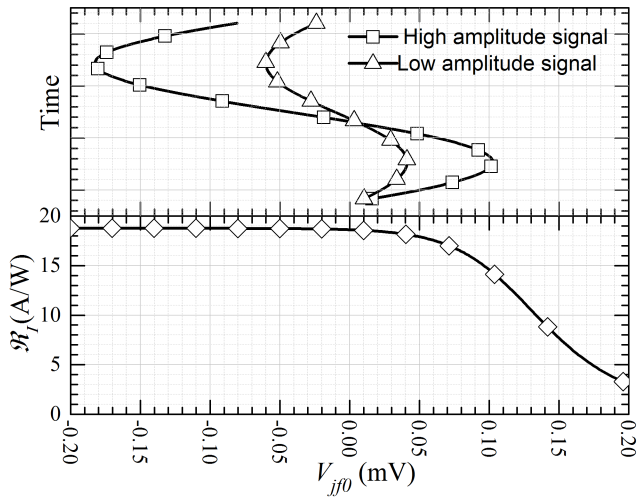

Fig. 3. Top: Two sine waves representing the voltage applied to the diode terminals. Bottom: Simulated current responsivity of the SMS7630 diode for a voltage sweep near the zero-bias condition.

factor. $\Re_{I0}$ is inversely proportional to N and has a maximum equal to 19.34 A/W at 300 K. This is the maximum current responsivity that any Schottky diode can reach at ambient temperature, thereby standing for an important limitation in the use of Schottky diodes for low-power energy harvesters. A recently published microwave power rectifier using heterojunction backward tunnel diodes with current responsivities on the order of 22 A/W has demonstrated how such a technology can be used to break through this Schottky diode limitation, thus greatly improving the MPH efficiency [14].

Equation (4) also depends on the external parameter V_{jf0}, decreasing when V_{jf0} increases and thus when the input power increases. This decrease in responsivity can be understood by looking at Fig. 3 where the simulated SMS7630 current responsivity is given together with two different amplitude V_j signals. The smaller amplitude signal remains in a maximum $\Re_I$ region. When the applied signal amplitude increases, the diode starts to operate in regions with a reduced $\Re_I$. If one thinks of the total $\Re_I^*$ as an average responsivity for the voltages through which the junction is excited, the average $\Re_I$ would then decrease with the increasing excitation signal amplitude. This variation of $\Re_I^*$ as a function of the external excitation is represented by $\Delta_{\Re}$ in (4) and is further explored in Section IV.

The current responsivity method can be used without $\Delta_{\Re_{I_0}}$ for low input power levels ranging up to a few microwatts of input power. The model becomes less accurate for an increasing power as the harmonics and dc bias in the diode junction voltage were ignored during the low power model derivation [4]. This range, however, is enough for ambient microwave energy harvesting aplications and can be extended using $\Delta_{\Re_{I_0}}$, as it will be further presented in Section IV.

Defining the RF-to-dc PCE as the total dc generated power divided by the power that reaches the junction, one can write the following equation:

$$\eta_{\mathrm{RFDC}} = \frac{P_{\mathrm{DC}}}{P_{jf0}} = \frac{R_j^2(I_{\mathrm{load}})}{R_L + R_s + R_j(I_{\mathrm{load}})} \cdot (\Re_{I_0} \cdot \Delta_{\Re_{I_0}})^2 \cdot P_{jf0}. \quad (5)$$

Equations (2) and (5) may be used to determine the optimum load value with which the maximum efficiency in the RF-to-dc PCE is reached. In Appendix A, it is shown that the load value for which the maximum efficiency is obtained is equal to $R_s + R_j(I_{\mathrm{load}})$. This can be simplifie to $R_j(I_{\mathrm{load}})$ within the square-law operation limits as R_s is much smaller than $R_j(I_{\mathrm{load}})$.

C. Parasitic Efficiency

Due to the low-pass filter effect of the diode's junction capacitance C_{j0}, some of the RF current that reaches the diode is shunted, thus dissipating power in the series resistance R_s. The total RF power that is delivered to the diode may be calculated by adding the power that reaches its junction to the power that is dissipated by the diode's series resistance R_s. The later may be calculated using the following equation, which can be derived using simple linear circuit theory:

$$P_{R_s} = \frac{1}{2} R_s \left| 2 \cdot \frac{P_{jf0}}{V_{jf0}} + i \cdot 2\pi \cdot f_0 \cdot C_{j0} \cdot V_{jf0} \right|^2. \quad (6)$$

The parasitic efficiency can be defined as the ratio between the total power supplied to the diode and the power that reaches the nonlinear junction, which may be expressed by

$$\eta_{\mathrm{parasitics}} = \frac{P_{jf0}}{P_{jf0} + P_{R_s}}. \quad (7)$$

Equations (6) and (7) can be simplified for the square-law low power region, where the junction resistance is considered to be constant and equal to R_{j0}, and the resulting equation is given in the following equation and was already given in [4] and [12]:

$$\eta_{\mathrm{parasitics}} = \frac{P_{jf0}}{P_{jf0} + P_{R_s}} = \left(\frac{1}{1 + (2\pi \cdot f_0 \cdot C_{j0})^2 \cdot R_{j0} \cdot R_s} \right)^2. \quad (8)$$

Equations (2), (5), and (7), which are used to calculate η_{SL}, η_{RFDC}, and $\eta_{\mathrm{parasitics}}$, respectively, describe the PCEs related to the diode parasitic components and nonlinearity. Assuming that the optimum load is chosen such that $\eta_{\mathrm{SL}} \cdot \eta_{\mathrm{RFDC}}$ is maximized, one can assume from (5) that diodes with higher R_j will reach higher efficiencies. In (8), however, the impact of a higher R_{j0} is seen to decrease efficiency. Finally, as it will be shown in the next session, the ZBR value also plays a key role in the matching network losses.

D. Matching Efficiency

The matching network insertion loss, or in turn, matching efficiency η_m, plays a significant role when determining the optimum diode for an ambient microwave power harvester. While (5) indicates that a diode with a high R_{j0} is expected to deliver a higher RF-to-dc PCE, it is shown that η_m is inversely proportional to R_{j0}. Using the given model, an optimum R_{j0} where $\eta_m \cdot \eta_{\mathrm{RFDC}} \cdot \eta_{\mathrm{SL}}$ is maximized can be suggested, indicating the optimum diode's zero-bias junction resistance.

A prior knowledge of the matching network technology in terms of transmission line attenuation and propagation

constants and lumped component quality factors can be used to estimate the matching efficie cy η_m as follows [15], [16]:

$$\eta_m = \frac{1}{1 + Q_r/Q_m} \tag{9}$$

$$Q_r = \sqrt{\frac{R_{\text{HIGH}}}{R_{\text{LOW}}} - 1} \tag{10}$$

where R_{HIGH} and R_{LOW} are the highest and lowest real impedances chosen from the source or the load, respectively, which are typically the antenna or source impedance and R_j, respectively, when matching a diode to an antenna. Q_r is called the required quality factor, while Q_m is the matching network quality factor that is actually obtained.

Finding the value of Q_m can be simplif ed by approximating the diode by a parallel $R_d//C_d$ circuit at the operation point of interest, which is determined by the input power and f_0. In this case, R_d is the equivalent parallel diode resistance to which the power is delivered and the equivalent parallel capacitance C_d will be absorbed into the matching network losses and bandwidth calculations. For a center frequency of interest, R_d and C_d may be calculated using the following equation, while maintaining the equivalent load quality factor [15]:

$$R_d = \text{Re}[Z_{\text{diode}}] \cdot \left(1 + Q_{\text{diode}}^2\right) \tag{11}$$

$$C_d = \left|\frac{\text{Im}[Z_{\text{diode}}]}{2\pi f_0}\right| \cdot \left(1 + Q_{\text{diode}}^{-2}\right) \tag{12}$$

where Z_{diode} is the input impedance of the diode alone at f_0 and the input power level of interest and Q_{diode} is the quality factor of the diode, calculated at the same frequency and power. For frequencies far below the diode cutoff frequency, it can be approximated by

$$Q_{\text{diode}} = \frac{\text{Im}[Z_{\text{diode}}]}{\text{Re}[Z_{\text{diode}}]}. \tag{13}$$

To obtain the quality factor of the matching network, its input impedance as a function of frequency $Z_{\text{match}}(f)$ needs to be calculated, with the f rst component of the matching network being C_d. Once this equation is known, Q_m may be calculated using one of the following two equations [17]:

$$Q_m(f) = \frac{1}{2}\frac{\text{Im}[Y_{\text{match}}(f)] + f\frac{d\text{Im}[Y_{\text{match}}(f)]}{df}}{\text{Re}[Y_{\text{match}}(f)]} \tag{14}$$

$$Q_m(f) = \frac{1}{2}\frac{\text{Im}[Z_{\text{match}}(f)] + f\frac{d\text{Im}[Z_{\text{match}}(f)]}{df}}{\text{Re}[Z_{\text{match}}(f)]} \tag{15}$$

where $Y_{\text{match}}(f)$ is the input admittance of the matching network, given by $1/Z_{\text{match}}(f)$. Equation (14) is used when the matching network behaves as a parallel resonator near f_0, while (15) is used when the behavior resembles a series resonator.

Every component used in the matching network's $Z_{\text{match}}(f)$ calculation needs to have its contributing parasitic parts included. When distributed transmission line components are used, the complex characteristic impedance of the line Z_c needs to be known. In [18], for example, it is shown that the quality factor of a short stub can vary by a factor of 2 if a simplif ed real impedance is used instead of the complex impedance of the transmission line.

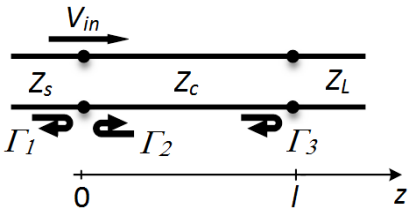

Fig. 4. Traveling wave approach used to calculate the standing wave ratio in a transmission line of length l.

When transmission lines are used as components of the matching network, it is important to take into account the effect that the standing waves have on losses. The increased voltage and current that appear on the line would introduce higher losses to the system. In [19], it is shown that an equivalent transmission line attenuation constant α_r can be calculated, which will account for these increased losses. α_r is related to the matched transmission line attenuation constant α_m by the following equation:

$$\alpha_r = \alpha_m \frac{r^2 + 1}{2r} \tag{16}$$

where r is the standing wave ratio sustained by the transmission line, which is usually calculated using the following equation, where Γ_L is the reflectio coeff cient at the load side:

$$r = \frac{1 + |\Gamma_L|}{1 - |\Gamma_L|}. \tag{17}$$

However, since transmission lines used in the design of matching networks are usually shorter than half-wavelength, it is not possible to assume that both maximum and minimum current and voltage nodes would appear in the standing wave sustained in the transmission line under consideration. For this reason, (17) cannot be used.

Using the traveling wave formulation, one can calculate the voltage at a short length of transmission line with reflecti n at both ends. Assuming a transmission line with propagation constant γ, characteristic impedance Z_c, and length l, connected to a source with impedance Z_S and a load with impedance Z_L, as shown in Fig. 4, one can write the voltage on the transmission line V_l as a function of the position z as given by

$$V_l(z) = V_{\text{in}}\begin{pmatrix} e^{-\gamma z} + \Gamma_3 e^{-2\gamma l}e^{\gamma z} + \Gamma_2\Gamma_3 e^{-2\gamma l}e^{-\gamma z} + \cdots \\ +\Gamma_2\Gamma_3^2 e^{-4\gamma l}e^{\gamma z} + \Gamma_2^2\Gamma_3^2 e^{-4\gamma l}e^{-\gamma z} + \cdots \end{pmatrix} \tag{18}$$

which can then be simplifie to (20) using (19)

$$\sum_{n=0}^{\infty} x^n = \frac{1}{1-x} \text{ for } |x| < 1 \tag{19}$$

$$V_l(z) = V_{\text{in}}\left[\frac{\left(e^{-\gamma z} + \Gamma_3 e^{\gamma z}e^{-2\gamma l}\right)}{1 - \Gamma_2\Gamma_3 e^{-2\gamma l}}\right]. \tag{20}$$

Using the points where the f rst derivative of (20) with respect to z equals 0, one can f nd the positions where $|V_l(z)|$ has a maximum or a minimum point. In Appendix B, it is

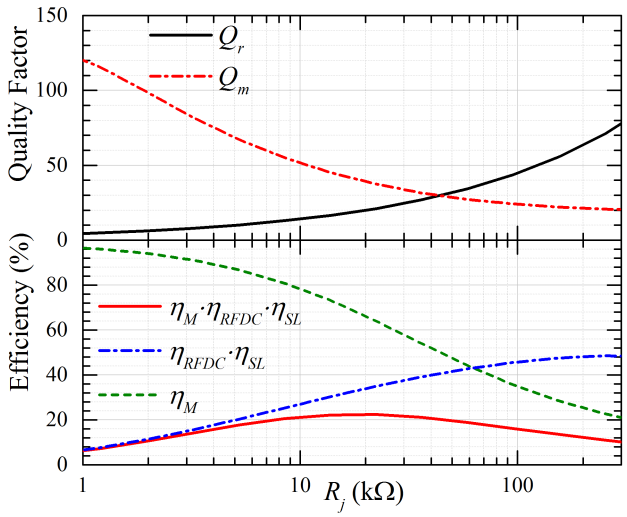

Fig. 5. Top: Calculated required quality factor Q_r and obtained matching network quality factor Q_m. Bottom: Calculated matching network efficiency, diode's η_{RFDC} η_{SL}, and the total efficiency at −30 dBm, 1.95 GHz. Load value equal to R_j.

shown that this happens for

$$z = \frac{n\pi + a\tan(-D/C)}{2\beta} \tag{21}$$

where β is the transmission line's phase constant, n is an integer equal or greater than 0, and C and D may be found from the following relationship: $\Gamma_3 \cdot \exp(-2\gamma l) = (C + D \cdot i)$.

If a z value is found to be within the limits of the transmission line length, a maximum or minimum standing voltage is found at this position. For short transmission lines, the maximum and minimum must standing voltages also be verified at the transmission line ends when less than two valid values of z are obtained from (21). Having the maximum and minimum standing wave voltages that occur within the transmission line boundaries, the following equation is used to calculate the maximum-to-minimum voltage ratio found in the transmission line:

$$r = \frac{|V_l(z)|_{\max}}{|V_l(z)|_{\min}}. \tag{22}$$

This value of r is used in conjunction with (16) to calculate the equivalent attenuation constant α_r for the transmission line, which is used to construct the $Z_{\mathrm{match}}(f)$ matching network input impedance equation.

Adding the matching network insertion loss effects to the microwave power rectification model gives the total tradeoff between the diode's junction resistance and the maximum microwave power rectification efficiency. Such a tradeoff is shown in Fig. 5 (bottom) for an input power equal to −30 dBm, using a hypothetical parasiticless diode. The rectifier power conversion efficiencies and insertion losses are calculated by considering that a microstrip L-Matching network is used, which is composed of a series transmission line and a parallel short-circuited stub, whose lengths are optimized to minimize reflections for every new value of R_j. A low-loss Rogers RT/Duroid 6002 substrate with a 30-mil thickness and a 18-μm copper cladding is used for the matching network insertion loss calculations. The microstrip line is 76 mil wide and the transmission line's propagation constant and complex characteristic impedance functions are extracted using the method proposed in [20]. This evaluation provides the range of junction resistances where the highest rectification efficiencies can be obtained using the proposed matching network. It is clear from this graph that for a parasiticless diode, a maximum could be obtained near 17 kΩ; however, close-to-the maximum efficiencies could be achieved with diodes that have an R_{j0} ranging from 5 up to 50 kΩ. The parasitic components will later reduce the maximum efficiency and play an important role in the maximum bandwidth that can be matched to the diode. This will be shown in the next section.

III. Wideband Energy Harvesting

The relationship between the load impedance and the maximum attainable matching bandwidth was described by Bode [21] and Fano [22], being known as the Bode–Fano criteria [23]. It gives the maximum bandwidth that can be matched to a load, given the load's equivalent circuit and the maximum desired reflection coefficient.

Usually, a carefully chosen bandwidth needs to be covered in microwave energy harvesting applications, over which the highest power densities are found.

Equation (23) can be used to calculate ΔB, the maximum obtainable fractional bandwidth that can be matched. It is derived using the Bode–Fano criterion for a parallel RC circuit

$$\Delta B \leq \frac{\pi}{R_d \cdot 2\pi f_0 C_d} \cdot \frac{1}{\ln \frac{1}{|\Gamma_{\mathrm{inband}}|}} \tag{23}$$

where f_0 is the frequency of interest, corresponding to the central frequency of the band, and Γ_{inband} is the desired reflection coefficient.

It is important to bear in mind that this equation is derived by assuming that the reflection coefficient is flat and equal to $|\Gamma_{\mathrm{inband}}|$ for the matched band and equal to one outside of this band. In this derivation, there are also other implicit assumptions, namely, the availability of lossless matching networks and wideband lossless impedance transformers. As one knows, matching networks always introduce losses to the system, and wideband impedance transformers are difficult to obtain over microwave frequency range for very different source and load impedances.

This means that in a real circuit design scenario, the maximum attainable bandwidth is actually lower than the calculated one by the Bode–Fano criteria, as such sharp transitions and flat passband are impossible to obtain. The out-of-band reflection coefficient will also not be equal to one for the whole frequency spectrum, thus reducing even further the maximum bandwidth that may be obtained.

However, the Bode–Fano criteria can be used to establish an upper bound to the maximum bandwidth that can be matched to a diode at a given frequency and estimated input power. In the comparisons below, it will be shown that despite that high R_{j0} diodes show an increased η_{RFDC} at low power level according to (5), the maximum bandwidth that can be matched to them is usually very narrow, as $R_d \propto R_{j0}$.

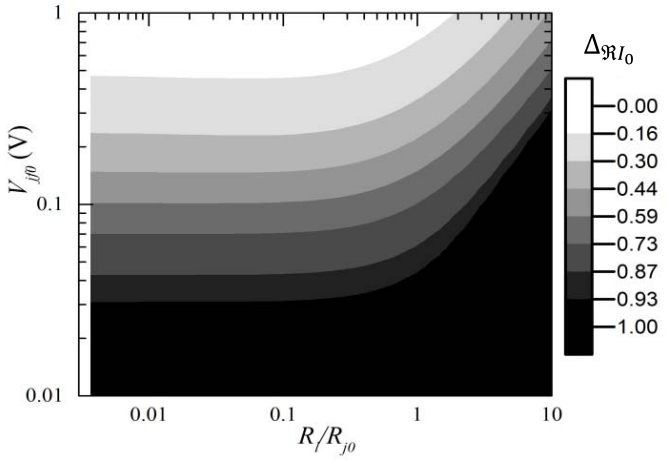

Fig. 6. $\Delta\Re$ contours for a theoretical diode model with infinit breakdown voltage. Curves were generated using the SMS7630 diode parameters.

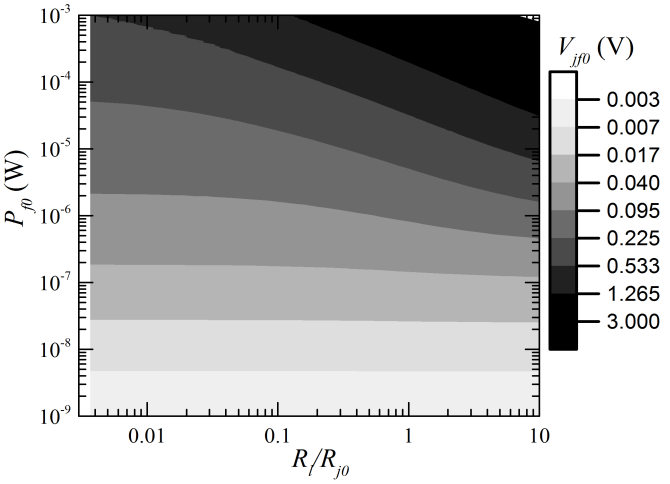

Fig. 7. Junction voltage as a function of the normalized load and of the input power for the SMS7630 diode.

IV. Extension of the Low-Power Model

The aforementioned method can be used to evaluate the RF-to-dc power conversion mechanism and understand where the power conversion inefficiencies take place. Even though the low-power model is limited in power to a few microwatts, this analysis can be extended to a larger power range by means of pregenerated V_{j0} as a function of the junction power and load resistor $V_{j0}(P_{jf0}, R_l)$, and current responsivity delta as a function of the junction voltage and normalized load $\Delta_{\Re}(V_{j0}, R_l/R_{j0})$ matrices, which are calculated with the aid of an harmonic balance algorithm implemented in MATLAB [24]. The $\Delta_{\Re}$ matrix contours are given in Fig. 6. These may be used for Schottky diodes operating below the breakdown voltage; however, the V_{j0} contours that are shown in Fig. 7 are diode dependent and need to be obtained for each different diode to be evaluated at higher input powers. All inductive and capacitive parasitic elements are removed during the contours generation to make them frequency independent. In this way, any further analysis may be done quickly and the results may be extrapolated to any frequency using only the previously presented linear equations. This procedure can be used to quickly evaluate and optimize microwave rectifiers at different frequencies or evaluate different matching network topologies.

The results of the extended method are compared with those of the low power model in the next section, where five commercial diodes are evaluated for a given MPH application. In addition to the insight into the power loss and power conversion mechanisms, the extended model is simpler and less resource consuming as all nonlinear dependences are already contained in the presented contours. Given these lower computational requirements, this method could be used to determine the optimum load in a maximum power point tracking algorithm embedded in the final dc–dc conversion stage.

V. Evaluation of Schottky Diodes Using the Proposed Method

The following commercially available Schottky diodes are selected and compared using the proposed method: Skyworks SMS7630, Infineon BAT15, Avago HSMS-2860, Avago HSMS-2850, and VDI W-Band ZBD. These diodes present very different saturation currents and R_{j0} within the boundaries given in Fig. 5, so the effects of a high, medium, or low barrier Schottky diode can be verified.

The proposed MPH operates in the GSM-1900 frequency band, covering from 1850 to 1990 MHz, as this is found to be one of the bands with a higher microwave power density in measurements done within the Poly-GRAMES research center environment. The operational input power range is optimized within the -45-to -30-dBm range. The load to which the power will be delivered is a 5.1-kΩ resistive load.

The matching network insertion losses were estimated even before defining the final matching network topology, and all rectifier calculations were done considering the use of a microstrip L-matching network composed of a series transmission line and a parallel short-circuited stub, which is also used as the dc current path. The same substrate and line impedances presented in Section II-D were used.

Using the proposed method and the diodes' characteristics given in the respective datasheets, the total RF-to-dc PCE and losses that take place in this conversion have been estimated. The result is given in Fig. 8 for the five proposed diodes. The results are organized from the diode with the highest R_{j0} on the top to the lowest R_{j0} at the bottom. The stacked areas are calculated with the extended model, using the pregenerated $V_{j0}(P_{jf0}, R_l)$ and $\Delta_{\Re I_0}(V_{j0}, R_l/R_{j0})$ matrices. The red triangles correspond to the model without the use of the deviation matrices.

The effect of variation of R_{j0} is obvious from the evaluation of Fig. 8, the first remarkable difference is the power dissipated by the matching network when higher barrier diodes are used, reaching 75% of the total power. This effect has already been shown and explained in Fig. 5, and is verified here again with real diode models. A higher R_{j0} also increases the total parasitic losses, as the low-pass filter effect from the parallel circuit composed of $R_j//C_j$ becomes more pronounced. This is true for low input power levels in the range of -30 dBm and lower, usually found in AMPH applications. At higher power levels, the decrease in R_j improves the matching and

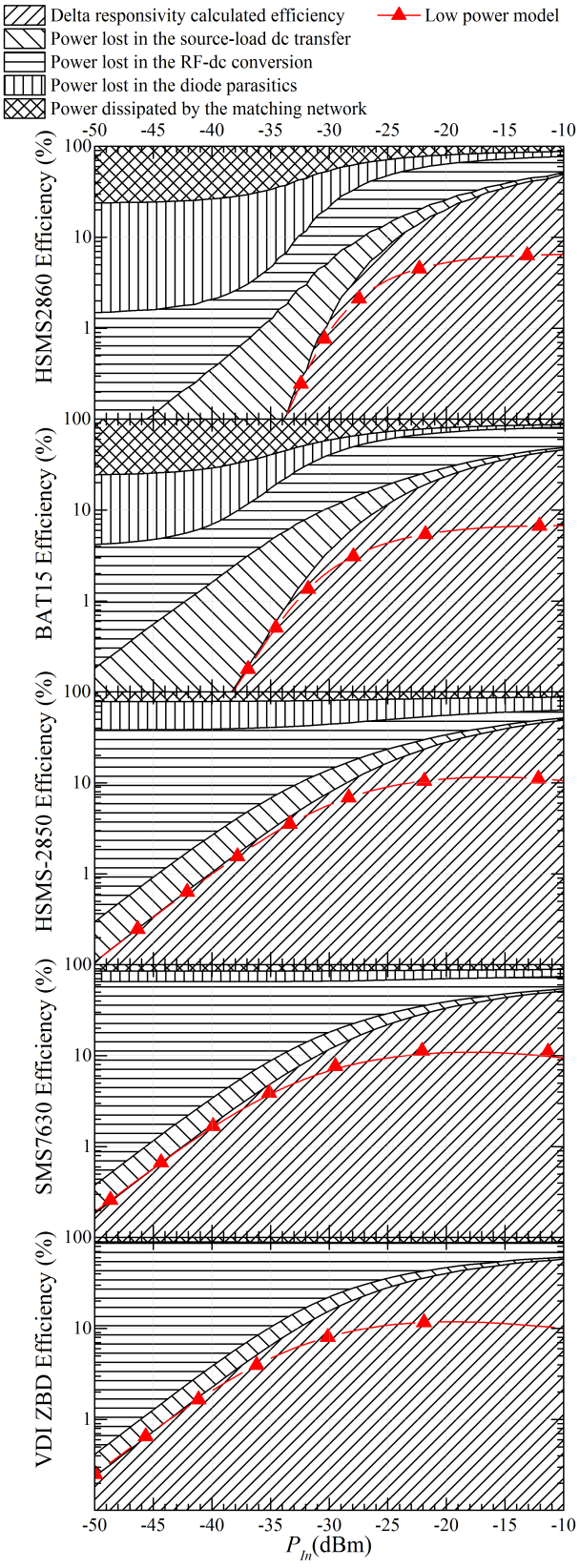

Fig. 8. RF-to-dc conversion efficiency for multiple diodes, where frequency = 1.9 GHz and load = 5.1 kΩ.

parasitic efficiencies, and unfortunately, this effect may not be explored in MPH because of the low ambient power densities that are available [3].

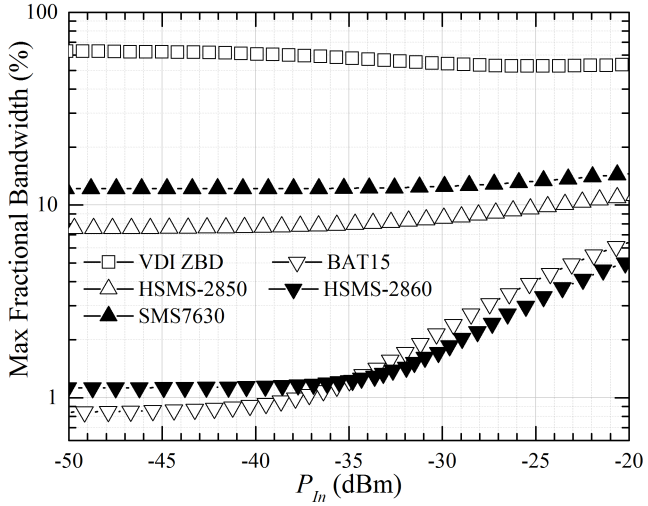

Fig. 9. Maximum obtainable fractional bandwidth for the proposed diodes, given a −12-dB return loss requirement.

The best predicted efficiencies are given by the low-barrier SMS7630 and VDI W-Band ZBD diodes, which present, respectively, 4.7% and 6.7% power conversion efficiencie at a −35-dBm input power level. Because of a higher C_{j0}, the HSMS-2850 diode dissipates nearly 40% of the available power in diode parasitic losses. The medium-to-high barrier height diodes, BAT15 and HSMS-2860, present two main limitations over this power region. First, the parasitic losses are very high. Second, because of the large R_j, nearly 75% of the power is dissipated in the matching network, even though the low-loss material Rogers RT/Duroid 6002 is used. Also as shown by (2), nearly all of the rectified power would be lost because of the low source-to-load power transfer efficiency in the proposed application. This last efficiency could be raised by increasing the load to a value near the diode's zero-bias junction resistance. Nevertheless, this would not reduce the high matching and parasitic losses problems. The maximum power that can be harvested with the higher barrier diodes in the square-law operation region can be calculated using the stacked area given by the recovered power efficiency and the source-to-load dc power transfer efficiency together with (2). The resulting maximum recoverable power is 50% of the value given by these two stacked areas if a load equal to R_{j0} is chosen. Having this in mind, Fig. 8 shows that the high-barrier diodes will not reach higher efficiencies even if a larger load is used in the AMPH power range.

Another limitation appears when studying the higher barrier diodes for low ambient power harvesting applications. As shown in Fig. 9, the maximum fractional bandwidth for the medium- and high-barrier diodes, calculated using (23), is below the minimum required fractional bandwidth of 7.4%.

One important remark about the Bode–Fano criteria is that it considers the fact that lossless matching networks and broadband impedance transformers are available at any frequency and for any source-load impedance mismatch [25]. Due to real component limitations, the realizable maximum bandwidth may be lower than that indicated in Fig. 9.

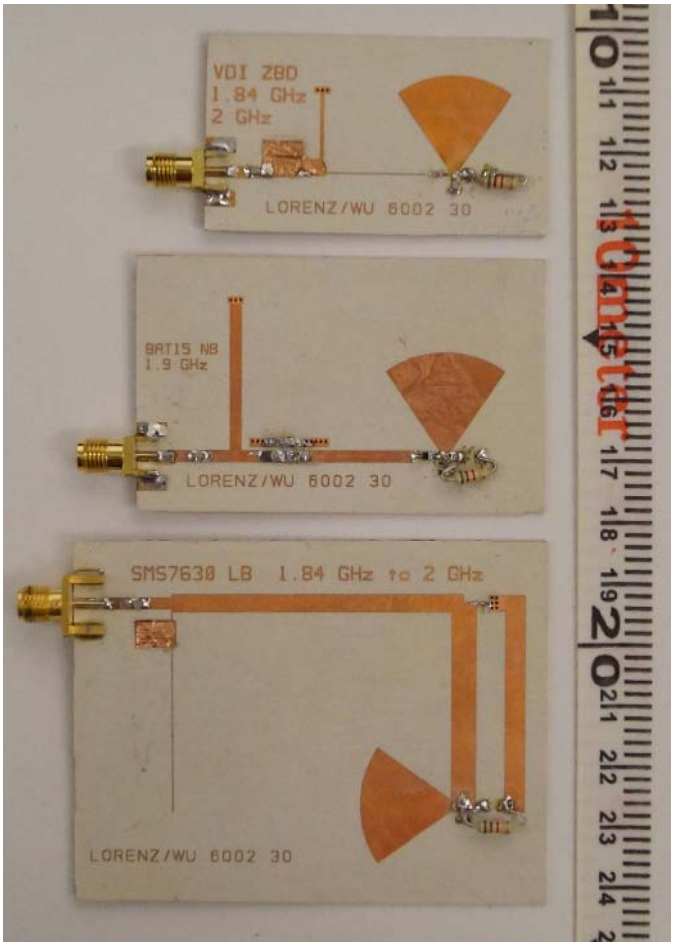

Fig. 10. Picture of the circuits built for this paper. Top: SMS7630. Middle: VDI ZBD. Bottom: BAT15.

VI. Measurement and Model Validation

In order to verify the proposed model, three prototypes were built using the power harvester specifications proposed in Section V. As shown in Fig. 9, the SMS7630-061 and the VDI W-Band ZBDs can be matched to the whole GSM-1900 frequency band when working at ambient RF power levels. Even though the HSMS-2850 diode could cover the whole bandwidth, it presents a lower efficiency leaving no margin for deviations. The higher barrier diodes do not comply with the bandwidth requirement and present lower RF-to-dc PCE due to high matching network insertion losses, nevertheless a third prototype using the BAT15 diode is presented to verify the model's predictions. The methodology used in this paper to build the prototypes is described hereunder and simplified in the flowchart given in Fig. 11.

1) After verifying parasitic losses, the diode's input impedance is calculated using the datasheet information and, when available, SPICE package parameters. The input power used during the matching circuit development is -35 dBm and the load is 5.1 kΩ.
2) An initial matching network, covering at least the frequency band ranging from 1.84 to 1.99 GHz is generated using the simplified real frequency technique [26], [27]. The minimum desired return loss is 12 dB.

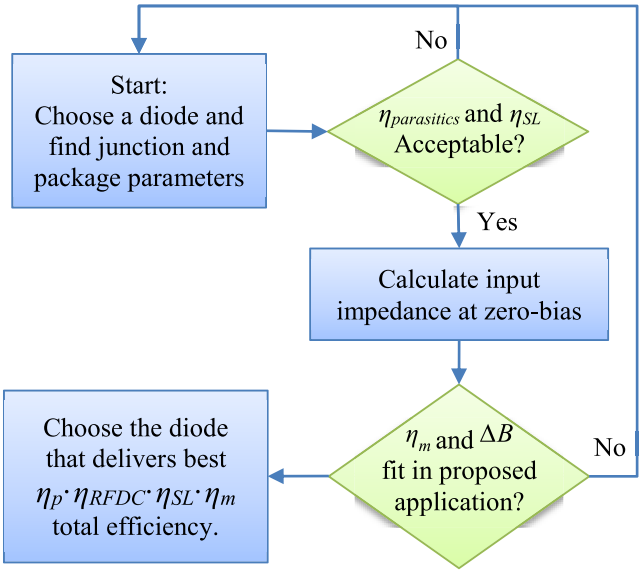

Fig. 11. Simplified flowchart on our proposed decision-making method to choose the optimum diode for a desired application. This can be used for low-power applications were R_j remains nearly unchanged.

3) The lumped components matching networks are converted into mixed and distributed matching networks, which are further optimized afterward using Keysight ADS LSSP and Momentum cosimulation.

The prototypes are then built using microstrip technology over a 30-mil Rogers RT/Duroid 6002 substrate, and the same substrate is used in the model calculations given in Fig. 8. A picture of the fabricated circuits is shown in Fig. 10.

For the efficiency measurement, the output of a RF generator is calibrated and then connected to the prototypes. The dc voltage $V_{\rm dc}$ over the output 5.1-kΩ load resistor is measured by an HP 34401A precision voltmeter. The measured efficiency is calculated using

$$\eta_{\rm meas} = \frac{V_{\rm dc}^2}{R_l \cdot P_{\rm in}}. \tag{24}$$

The simulated and measured S_{11} for a -35 dBm input signal, as well as the measured and calculated power conversion efficiencies for a -30 dBm input signal, are shown in Fig. 12.

The maximum bandwidth for a return loss of -12 dB, calculated using the Bode–Fano criteria, is shown as a grayed out area. The obtained bandwidths are near-to-the maximum predicted value, considering that the measured return loss is lower than -12 dB for some frequencies, and not flat as considered in the Bode–Fano criteria derivations.

As shown in the results, the agreement between the simulated and measured S_{11} is very good for the SMS7630 and BAT15 diodes. However, a difference is observed between the initially simulated and measured S_{11} values for the VDI prototype. This happened mainly because of a large tolerance that this diode presents for the value of I_s, reflecting on a junction resistance that may vary from 2.5 to 6 kΩ. It was initially assumed in this work an I_s value equal to 11 μA; however, from the measurements, it was found that the used sample presents an I_s near 7 μA. The measured S_{11} values presented in Fig. 12 are obtained after tuning the matching network, which was done using a copper tape as can be seen

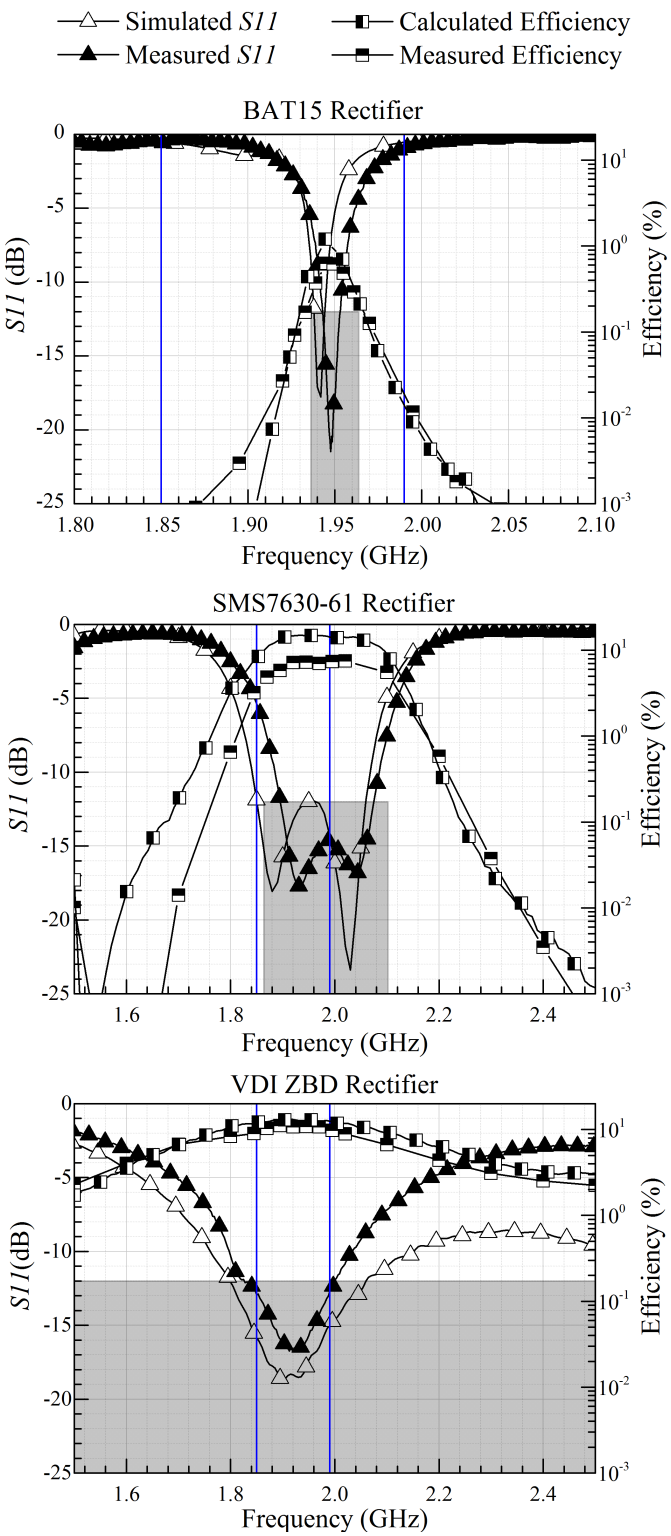

Fig. 12. Measured and calculated S_{11} (at −35 dBm) and PCE (at −30 dBm). The theoretical maximum bandwidth for a −12 dB-return loss is indicated by the grayed out area. The proposed prototype bandwidth is indicated by the parallel blue line.

in Fig. 10. Tuning was needed mainly to bring the matched frequency band to the desired values—slight initial detuning was expected as the diode parameters given in the datasheet was used instead of an accurate model.

The measured power conversion efficiencies agree very well with the values predicted by the model, which are calculated using the $\Delta_{\Re I_0}$ extended mathematical model. η_m is calculated using the measured reflection coefficient and the matching network insertion loss, estimated using Keysight ADS Momentum software package, as the wider band matching networks become too complicated to be modeled mathematically.

After the bandwidth measurement, a power sweep is done to verify the model PCE prediction at different power levels. The power distribution, calculated using the $\Delta_{\Re I_0}$ model is shown in Fig. 13 for the three built prototypes, together with the measured results. A very good agreement between the model predictions and measurements is found and verified for the BAT15 and VDI prototypes. A small difference is observed between the measured and predicted power conversion efficiencies of the SMS7630, this difference shown in Figs. 12 and 13 is believed to be the result of an underestimation of the diode model parasitic components, or in the diode package parasitic components.

As expected from the previous discussions, the higher initial mismatch between the source and the load for the diodes with higher R_{j0} results in a very high loss of P_{in} in connection with the increased matching network insertion losses. For the SMS7630 diode, this loss accounts for 18% of P_{in}, while for the BAT15 diode, this raises to nearly 82% of P_{in}. The increase in the matching network insertion losses for the BAT15 prototype, compared with the predictions given in Fig. 8, is mainly caused by the use of a longer transmission line between the diode and the parallel capacitor, compared with the transmission line used with a parallel shorted stub solution, which allows a larger standing wave ratio to be sustained, increasing the losses.

Despite the fact that the SMS7630 diode has a slightly higher R_j than the VDI ZBD, the larger diode parasitic losses decrease the final efficiency, as nearly 18.8% of the total input power is lost in the diode's parasitic components. This results in a total efficiency very near for both rectifiers, with the VDI ZBD rectifier delivering the best performance: 11.2% at −30 dBm compared with 8% measured on the SMS7630 rectifier.

VII. Discussion

Fig. 14 shows a comparison between the two discussed models: the low power model reviewed in the beginning of this paper and the extended low power model described in Section IV. The matching efficiency, even though very important in the total harvesting process as proved already, could not be added as all previously published models did not include it. The power ranges and scenarios where each method delivers the best results could be highlighted, these models are the diode operating as a switch [13] and the Ritz–Galerkin solution for the diode non-linear equations [28]. The Keysight ADS harmonic balance result was added as reference.

The limitation in the low-power models for higher input powers is evident from Fig. 14. Nevertheless, the result at input power levels up to a few microwatts makes the low power model a very good tool to predict the performance of AMPH devices. The delta-responsivity matrix model delivers

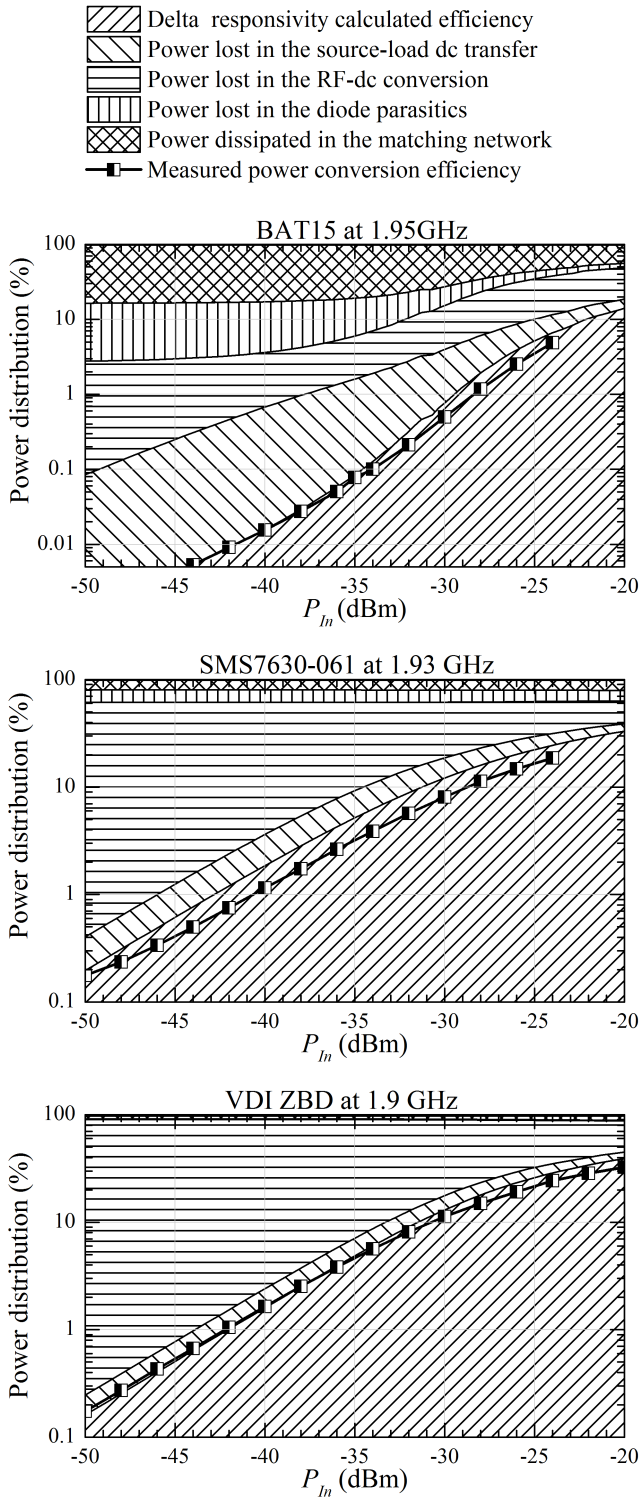

Fig. 13. Measured and calculated MPH efficiencies with power distribution. $f = 1.9$ GHz and load $= 5.1$ kΩ.

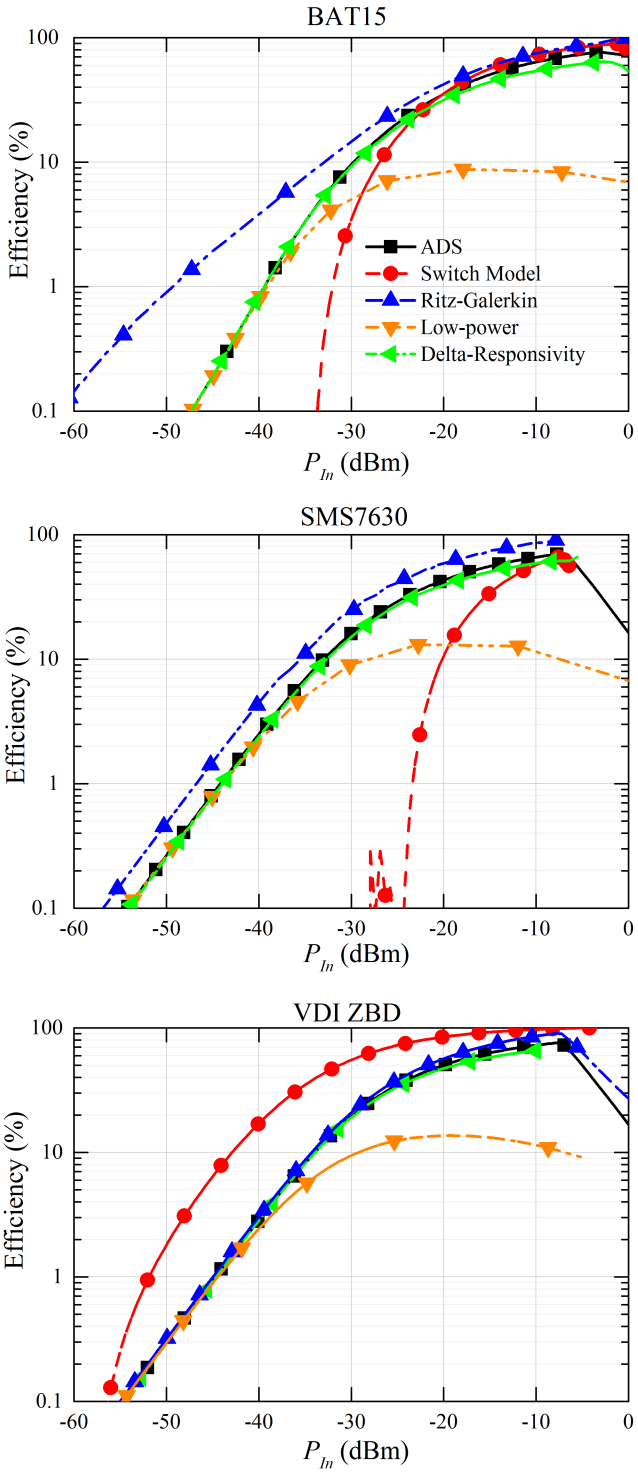

Fig. 14. Comparison of the predictions given by the proposed methods and other already published models. Matching network insertion losses are not included as other models do not include them. $f = 1.9$ GHz and a 5.1-kΩ load.

an exact result compared with the Keysight ADS simulation results, even at higher input power levels. The Ritz–Galerkin model has a shift up in the efficiency for the SMS7630 and the BAT15 diodes, as a result of simplification in the model derivation where the parasitic capacitances are ignored. This effect is not seen for the VDI ZBD due to its very low parasitic capacitances. As expected, the switch diode model works well for higher input powers and higher R_{j0} diodes, as is seen in the BAT15 diode results, but cannot be used in the case of low-power levels related to AMPH applications.

The application of the Bode–Fano criteria for an AMPH device has also been demonstrated, predicting correctly which diodes may be matched to the desired frequency band of

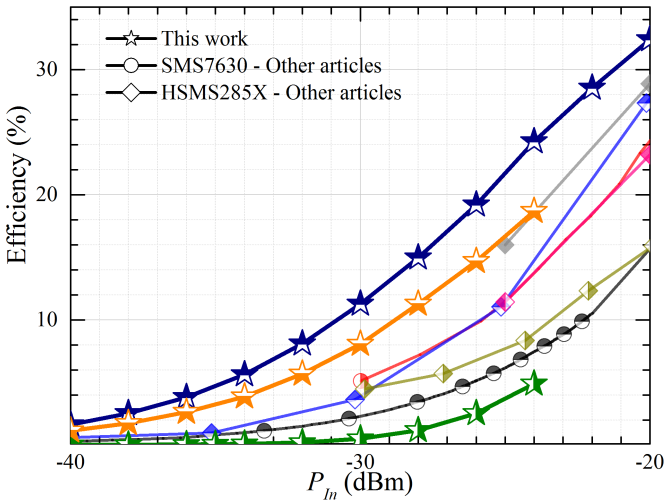

Fig. 15. Comparison of the measured rectifiers' efficiencies with those of other state-of-the-art microwave rectifiers. The references are given in Table I.

TABLE I

LIST OF RECTIFIERS PRESENTED IN FIG. 15

Symbol	Year	Diode	Frequency	Reference
	2015	VDI ZBD	1.9 GHz	Prototype
	2015	SMS7630	1.9 GHz	Prototype
	2015	BAT15	1.9 GHZ	Prototype
	2010	SMS7630	2.45 GHz	[29]
	2014	SMS7630	2.45 GHz	[30]
	2013	HSMS2855	2.45 GHz	[31]
	2012	HSMS285X	1.8 GHz	[32]
	2014	HSMS285X	1.8 GHz	[33]
	2014	HSMS285X	2.1 GHz	[33]

operation.

Based on the presented results, the authors suggest that in order to increase efficiency of low-power microwave energy harvesters, there are mainly two paths that still need to be further investigated. The first is the use of devices with higher current responsivity than Schottky diodes, as is the case of recently published results on backward heterojunction tunnel diodes [3], [5], [34]. The second path is the improvement in matching network quality factor. As shown in [35], a power harvester working at 13.56 MHz has achieved nearly 55% of efficiency at a −30-dBm input power, using quartz crystals in the matching network, although this approach results in narrower bandwidths.

In Fig. 15, the prototypes' measured power conversion efficiencies are compared with some of the state-of-the-art MPH published results. Only the results from rectifiers using Schottky diodes with matching network losses included in the efficiency measurements are plotted. Published papers that report results in frequencies below 1 GHz or above 4 GHz are not considered to keep parasitic losses within the same range. It may be seen that the result presented in [33] is very close to the performance obtained by the prototype using the SMS7630 diode. This is expected as the dc load used in both works had similar values and both diodes present similar characteristics. As far as the authors are aware, the efficiency presented by the prototype using the VDI ZBD is the highest published within the power range of interest using Schottky diodes for rectification, being close to the latest results presented for CMOS rectifiers [36] at the 1.9-GHz frequency range.

VIII. CONCLUSION

In this paper, a mathematical model has been presented and verified, in which the Schottky diode microwave power harvesting efficiency-related physical mechanisms are explained and formulated. A mathematical process that can correctly predict the matching network insertion loss impact on the total AMPH efficiency has been incorporated into the microwave energy harvesting model for the first time. It has been shown that matching network losses can account for as high as 82% of the total input power losses being of fundamental importance when studying the AMPH.

Knowing where the power is dissipated enables the design and development of a new class of rectifier with maximized conversion efficiency. The modeled efficiencies, calculated in conjunction with the matching network losses, are in close agreement with the measured results. Even though the matching network insertion losses are approximated by a simpler L-matching network, the results show good agreement with the final wider band matching network calculated and measured results, thus substantiating the claim that the proposed model can be used as a trustworthy approximation of the maximum attainable power conversion efficiencies, even before having the rectifier circuit designed.

APPENDIX A

The mathematical proof of the optimum load where the maximum PCE is obtained is shown in the following equation, and this is valid for the low input power range explored in this work, usually while the diode is operating in the square-law region. From (2) and (5), one can write

$$\eta_{\mathrm{SL}} \cdot \eta_{\mathrm{RFDC}} = \frac{K \cdot R_L \cdot R_j^2}{(R_L + R_S + R_j)^2} \tag{25}$$

where $K = (\Re_{I0} \cdot \Delta_{\Re_{I0}})^2 \cdot P_{jf0}$. The first derivative of this equation as a function of the load R_L is shown as follows:

$$\frac{\partial(\eta_{\mathrm{SL}} \cdot \eta_{\mathrm{RFDC}})}{\partial R_L} = \frac{K \cdot R_j^2 \cdot (R_L + R_S + R_j) - 2K \cdot R_L \cdot R_j^2}{(R_L + R_S + R_j)^2}. \tag{26}$$

Making it equal to 0, one can find the values of R_L where $\eta_{\mathrm{SL}} \cdot \eta_{\mathrm{RFDC}}$ has a maximum or a minimum

$$\begin{aligned} K \cdot R_j^2 \cdot (R_L + R_S + R_j) - 2K \cdot R_L \cdot R_j^2 &= 0 \\ R_j^2 \cdot R_S + R_j^3 &= R_L \cdot R_j^2 \\ R_L &= R_S + R_j. \end{aligned} \tag{27}$$

As the second derivative of $\eta_{\mathrm{SL}} \cdot \eta_{\mathrm{RFDC}}$ is always negative, this point represents the only maximum of $\eta_{\mathrm{SL}} \cdot \eta_{\mathrm{RFDC}}$, which happens when the load is equal to the diode resistance (which can be approximated by R_j at low power level).

APPENDIX B

In order to find the z positions where (26) has a minimum voltage amplitude or a maximum voltage amplitude, its first derivative is calculated by

$$\frac{\partial |V_l(z)|}{\partial z} = \left| \frac{V_{\text{in}}}{1 - \Gamma_2 \Gamma_3 e^{-2\gamma l}} \right| \cdot \frac{\partial |(e^{-\gamma z} + \Gamma_3 e^{\gamma z} e^{-2\gamma l})|}{\partial z}. \quad (28)$$

Making $C + iD = \Gamma_3 \cdot e^{-2\gamma l}$ to simplify the mathematical derivation

$$\frac{\partial |V_l(z)|}{\partial z} = \left| \frac{V_{\text{in}}}{1 - \Gamma_2 \Gamma_3 e^{-2\gamma l}} \right| \cdot \frac{\partial |[e^{-\gamma z} + (C + iD) e^{\gamma z}]|}{\partial z}. \quad (29)$$

One can use the points where this equation is equal to zero so as to find the candidate maximum and minimum standing wave voltage amplitude positions

$$\begin{aligned} &\frac{\partial |[e^{-\gamma z} + (C + iD) e^{\gamma z}]|}{\partial z} \\ &\quad = \frac{\partial \sqrt{[(C+1)\cos(\beta z) - D \sin(\beta z)]^2}}{\partial z} \\ &\qquad + \frac{\partial \sqrt{[D \cos(\beta z) + (C-1)\sin(\beta z)]^2}}{\partial z} \\ &\quad = 0. \end{aligned} \quad (30)$$

Expanding these equations and simplifying the resulting expression using trigonometric identities, one can get

$$C \sin(2\beta z) + D \cos(2\beta z) = 0 \quad (31)$$

which finally results in the previously given result equal to

$$z = \frac{n \cdot \pi + \operatorname{atan}\left(-\frac{D}{C}\right)}{2\beta} \quad (32)$$

where n is any integer number equal or larger than zero.

ACKNOWLEDGMENT

The authors would like to thank Rogers Corporation and Virginia Diodes, which provided the samples, which were of great importance during the development of this paper. The authors would also like to thank J. Gauthier, D. Dousset, M. Thibault, S. Dubé, T. Antonescu, and J.-S. Décarie of the Poly-Grames Research Center, Ecole Polytechnique de Montreal, for their technical assistance.

REFERENCES

[1] W. C. Brown, "Experimental airborne microwave supported platform," Rome Air Develop. Center, Rome, NY, USA, Tech. Rep. RADC-TR-65-188, Dec. 1965.

[2] R. M. Dickinson, "Performance of a high-power, 2.388-GHz receiving array in wireless power transmission over 1.54 km," in *IEEE MTT-S Int. Microw. Symp. Dig.*, New York, NY, USA, Jun. 1976, pp. 139–141.

[3] S. Hemour and K. Wu, "Radio-frequency rectifier for electromagnetic energy harvesting: Development path and future outlook," *Proc. IEEE*, vol. 102, no. 11, pp. 1667–1691, Nov. 2014.

[4] S. Hemour *et al.*, "Towards low-power high-efficiency RF and microwave energy harvesting," *IEEE Trans. Microw. Theory Techn.*, vol. 62, no. 4, pp. 965–976, Apr. 2014.

[5] C. H. P. Lorenz *et al.*, "Overcoming the efficiency limitation of low microwave power harvesting with backward tunnel diodes," in *IEEE MTT-S Int. Microw. Symp. Dig.*, Phoenix, AZ, USA, May 2015, pp. 1–4.

[6] M. Pinuela *et al.*, (2012). *London RF Survey*, accessed on Jun. 14, 2014. [Online]. Available: http://www.londonrfsurvey.org/

[7] F. Giuppi, K. Niotaki, A. Collado, and A. Georgiadis, "Challenges in energy harvesting techniques for autonomous self-powered wireless sensors," in *Proc. Eur. Microw. Conf.*, 2013, pp. 854–857.

[8] J. G. Koomey, S. Berard, M. Sanchez, and H. Wong, "Implications of historical trends in the electrical efficiency of computing," *IEEE Annu. Hist. Comput.*, vol. 33, no. 3, pp. 46–54, Mar. 2011.

[9] J. G. Koomey, H. S. Matthews, and E. Williams, "Smart everything: Will intelligent systems reduce resource use?" *Annu. Rev. Environ. Resour.*, vol. 38, pp. 311–343, Oct. 2013.

[10] Libelium. (2015). *50 Sensor Applications for a Smarter World*, accessed on Jun. 15, 2015. [Online]. Available: http://www.libelium.com/top_50_iot_sensor_applications_ranking/

[11] T.-W. Yoo and K. Chang, "Theoretical and experimental development of 10 and 35 GHz rectennas," *IEEE Trans. Microw. Theory Techn.*, vol. 40, no. 6, pp. 1259–1266, Jun. 1992.

[12] H. C. Torrey, C. A. Whitmer, and S. A. Goudsmit, *Crystal Rectifiers*, 1st ed. New York, NY, USA: McGraw-Hill, 1948.

[13] J. Guo and X. Zhu, "An improved analytical model for RF-DC conversion efficiency in microwave rectifiers," in *IEEE MTT-S Int. Microw. Symp. Dig.*, Montreal, QC, Canada, Jun. 2012, pp. 1–3.

[14] C. H. P. Lorenz *et al.*, "Breaking the efficiency barrier for ambient microwave power harvesting with heterojunction backward tunnel diodes," *IEEE Trans. Microw. Theory Techn.*, vol. 63, no. 12, pp. 4544–4555, Dec. 2015.

[15] A. M. Niknejad, *Electromagnetics for High-Speed Analog and Digital Communication Circuits*. New York, NY, USA: Cambridge Univ. Press, 2007.

[16] C. H. P. Lorenz, S. Hemour, and K. Wu, "Modeling and influence of matching network insertion losses on ambient microwave power harvester," in *Proc. IEEE MTT-S Int. Conf. Numer. Electromagn. Multiphys. Modeling Optim.*, Ottawa, ON, Canada, Aug. 2015, pp. 1–3.

[17] P. Vizmuller, *RF Design Guide: Systems, Circuits and Equations*, vol. 1. Norwood, MA, USA: Artech House, 1995.

[18] A. R. Djordjevic, A. G. Zajic, D. V. Tosic, and T. Hoang, "A note on the modeling of transmission-line losses," *IEEE Trans. Microw. Theory Techn.*, vol. 51, no. 2, pp. 483–486, Feb. 2003.

[19] G. L. Ragan, *Microwave Transmission Circuits*, vol. 9. New York, NY, USA: Boston Technical Publishers, 1964.

[20] J. E. Zúñiga-Juárez, A. Reynoso-Hernández, M. del Carmen Maya-Sánchez, and R. S. Murphy-Arteaga, "A new analytical method to calculate the characteristic impedance Z_C of uniform transmission lines," *Computación y Sistemas*, vol. 16, no. 3, pp. 277–285, 2012.

[21] H. W. Bode, *Network Analysis & Feedback Amplifier Design*. New York, NY, USA: Van Nostrand, 1945.

[22] R. M. Fano, "Theoretical limitations on the broadband matching of arbitrary impedances," *J. Franklin Inst.*, vol. 249, no. 2, pp. 139–154, 1950.

[23] D. M. Pozar, *Microwave and RF Wireless Systems*. New York, NY, USA: Wiley, 2001.

[24] S. A. Maas, *Microwave Mixers*, 2nd ed. Boston, MA, USA: Artech House, 1993.

[25] J. L. Hesler and B. Gelmont, "A discussion of power coupling bandwidth limitations of planar Schottky diodes at submillimeter wavelengths," in *Proc. 19th Int. Symp. Space Teraherz Technol.*, Mar. 1998, pp. 173–180.

[26] B. S. Yarman, *Design of Ultra Wideband Antenna Matching Networks: Via Simplified Real Frequency Technique*. Dordrecht, The Netherlands: Springer, 2008.

[27] B. S. Yarman, *Design of Ultra Wideband Power Transfer Networks*. West Sussex, U.K.: Wiley, 2010.

[28] R. G. Harrison, "Full nonlinear analysis of detector circuits using Ritz–Galerkin theory," in *IEEE MTT-S Int. Microw. Symp. Dig.*, vol. 1. Albuquerque, NM, USA, Jun. 1992, pp. 267–270.

[29] G. A. Vera, A. Georgiadis, A. Collado, and S. Via, "Design of a 2.45 GHz rectenna for electromagnetic (EM) energy scavenging," in *Proc. IEEE Radio Wireless Symp.*, New Orleans, LA, USA, Jan. 2010, pp. 61–64.

[30] W. Haboubi *et al.*, "An efficient dual-circularly polarized rectenna for RF energy harvesting in the 2.45 GHz ISM band," *Prog. Electromagn. Res.*, vol. 148, pp. 31–39, 2014.

[31] B. R. Franciscatto, V. Freitas, J.-M. Duchamp, C. Defay, and T. P. Vuong, "High-efficiency rectifier circuit at 2.45 GHz for low-input-power RF energy harvesting," in *Proc. Eur. Microw. Conf.*, Oct. 2013, pp. 507–510.

[32] V. Marian, B. Allard, C. Vollaire, and J. Verdier, "Strategy for microwave energy harvesting from ambient field or a feeding source," *IEEE Trans. Power Electron.*, vol. 27, no. 11, pp. 4481–4491, Nov. 2012.

[33] Z. Liu, Z. Zhong, and Y.-X. Guo, "High-efficien y triple-band ambient RF energy harvesting for wireless body sensor network," in *Proc. IEEE MTT-S Int. Microw. Workshop. Ser. RF Wireless Technol. Biomed. Healthcare Appl.*, London, U.K., Dec. 2014, pp. 1–3.
[34] Z. Zhang, R. Rajavel, P. Deelman, and P. Fay, "Sub-micron area hetero-junction backward diode millimeter-wave detectors with 0.18 pW/Hz$^{1/2}$ noise equivalent power," *IEEE Microw. Wireless Compon. Lett.*, vol. 21, no. 5, pp. 267–269, May 2011.
[35] A. Nimo, D. Grgić, T. Ungan, and L. M. Reindl, "A new family of passive wireless RF harvesters based on R-C-Quartz oscillators," in *Proc. Eur. Microw. Conf.*, Oct. 2013, pp. 511–514.
[36] C. R. Valenta and G. D. Durgin, "Harvesting wireless power: Survey of energy-harvester conversion eff ciency in far-f eld, wireless power transfer systems," *IEEE Microw. Mag.*, vol. 15, no. 4, pp. 108–120, Jun. 2014.

Carlos Henrique Petzl Lorenz received the Dipl.-Ing. degree in electrical engineering from the Federal University of Technology–Paraná, Curitiba, Brazil, in 2007, and the master's degree from the École Polytechnique de Montréal, Montréal, QC, Canada, in 2015.

He was a Research and Development Engineer with Landis+Gyr Brazil, Curitiba, from 2007 to 2013, where he was involved in the development of wireless communication interfaces. In 2013, he joined the Poly-Grames Research Center, École Polytechnique de Montréal, where he stayed until 2015. He is currently with the satellite industry. His current research interests include microwave energy harvesting, power conversion and generation for low-power systems, passive intermodulation, and multipactor effect.

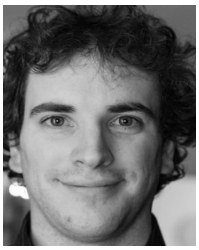

Simon Hemour (S'08–M'11–SM'16) received the B.S. degree in electrical engineering from the University of Grenoble, Grenoble, France, in 2004, and the M.S. and Ph.D. degrees in optics, optoelectronics, and microwave engineering from the Grenoble Institute of Technology, Grenoble, France, in 2006 and 2010, respectively.

He was with the European Organization for Nuclear Research, Geneva, Switzerland, in 2003, as a part of the Instrumentation Department, where he was involved with the ATLAS experiment on the Large Hadron Collided. From 2006 to 2007, he was a Research Assistant with the Pidstryhach Institute of Applied Problems of Mechanics and Mathematics (IAPMM), National Academy of Science of Ukraine (NASU), Lviv, Ukraine. In 2007, he joined the IMEP-LAHC MINATEC Laboratory, Grenoble, France. From 2011 to 2015, he was with the Poly-Grames Research Center, École Polytechnique de Montréal, Montréal, QC, Canada, where he was leading the Wireless Power Transmission and Harvesting Research Group. He joined the University of Bordeaux, Bordeaux, France, in 2015, where is currently an Associate Professor. There he leads research in wireless micro energy solutions for IoT and biomedical applications. His current research interests include wireless power transfer and hybrid energy harvesting, nonlinear devices, innovative RF measurements, RF interferometry, low-power microwave, and millimeter-wave conversion circuits.

Dr. Hemour is a Member of the IEEE MTT-26 Wireless Energy Transfer and Conversion Technical Committee.

Ke Wu (M'87–SM'92–F'01) received the B.Sc. (Hons.) degree in radio engineering from Southeast University, Nanjing, China, in 1982, and the D.E.A. and Ph.D. (Hons.) degrees in optics, optoelectronics, and microwave engineering from the Institut National Polytechnique de Grenoble, Grenoble, France, and the University of Grenoble, Grenoble, France, in 1984 and 1987, respectively.

He is currently a Professor of Electrical Engineering, and a Tier-I Canada Research Chair in RF and millimeter-wave engineering with the École Polytechnique de Montréal, Montréal, QC, Canada. He is also the NSERC Industrial Research Chair in future wireless technologies. He has been the Director of the Poly-Grames Research Center. He was the Founding Director of the Center for Radiofrequency Electronics Research of Quebec (Regroupement stratégique of FRQNT). He has also held guest, visiting, and honorary professorships at many universities around the world. He has authored or co-authored over 1000 referred papers and a number of books/book chapters and has f led over 40 patents. His current research interests include substrate integrated circuits, antenna arrays, advanced CAD and modeling techniques, wireless power transmission and harvesting, and development of low-cost RF and millimeter-wave transceivers and sensors for wireless systems and biomedical applications. He is also interested in the modeling and design of microwave and terahertz photonic circuits and systems.

Dr. Wu is a Member of the Electromagnetics Academy, Sigma Xi Honorary Society, and International Union for Radio Science. He is a Fellow of the Canadian Academy of Engineering and of the Royal Society of Canada (The Canadian Academy of the Sciences and Humanities). He was a recipient of many awards and prizes, including the f rst IEEE MTT-S Outstanding Young Engineer Award, the 2004 Fessenden Medal of the IEEE Canada, the 2009 Thomas W. Eadie Medal of the Royal Society of Canada, the Queen Elizabeth II Diamond Jubilee Medal in 2013, the 2013 FCCP Education Foundation Award of Merit, the 2014 IEEE MTT-S Microwave Application Award, the 2014 Marie-Victorin Prize (Prix du Quebec—the highest distinction of Québec in the natural sciences and engineering), the 2015 Prix d'Excellence en Recherche et Innovation of Polytechnique Montréal, and the 2015 IEEE Montreal Section Medal of Achievement. He is the inaugural three-year representative of North America as a Member of the European Microwave Association General Assembly. He was an IEEE Microwave Theory and Techniques Society Distinguished Microwave Lecturer from 2009 to 2011. He is the 2016 IEEE Microwave Theory and Techniques Society President. He is an elected IEEE Microwave Theory and Techniques Society AdCom Member from 2006 to 2015 and served as Chair of the IEEE Microwave Theory and Techniques Society Transnational Committee, Member and Geographic Activities Committee and Technical Coordinating Committee among many other AdCom functions. He is currently the Chair of the joint IEEE chapters of MTTS/APS/LEOS in Montréal. He has held key positions in and has served on various panels and international committees, including the Chair of Technical Program Committees, the international Steering Committees, and international conferences/symposia. He was the General Chair of the 2012 IEEE Microwave Theory and Techniques Society International Microwave Symposium. He has served on the editorial/review boards of many technical journals, transactions, proceedings, and letters and scientif c encyclopedia including as an Editor and Guest Editor.